Inorganic Chemistry

Article

pubs.acs.org/IC

Reversible Deprotonation and Protonation Behaviors of a Tetra-Protonated γ-Keggin Silicodecatungstate

Kosei Sugahara, Shinjiro Kuzuya, Tomohisa Hirano, Keigo Kamata, and Noritaka Mizuno*

Department of Applied Chemistry, School of Engineering, The University of Tokyo, 7-3-1 Hongo, Bunkyo-ku, Tokyo 113-8656, Japan

Supporting Information

ABSTRACT: The potentiometric titration of a γ-Keggin tetra-protonated silicodecatungstate, $[\gamma\text{-}SiW_{10}O_{34}(H_2O)_2]^{4-}$ (H_4·**I**), with TBAOH (TBA = $[(n\text{-}C_4H_9)_4N]^+$) showed inflection points at 2 and 3 equiv of TBAOH. The ^1H, ^{29}Si, and ^{183}W NMR data suggested that the in situ formation of tri-, doubly-, and monoprotonated silicodecatungstates, $[\gamma\text{-}SiW_{10}O_{34}(OH)(OH_2)]^{5-}$ (H_3·**I**), $[\gamma\text{-}SiW_{10}O_{34}(OH)_2]^{6-}$ (H_2·**I**), and $[\gamma\text{-}SiW_{10}O_{35}(OH)]^{7-}$ (H·**I**), with C_1, C_{2v}, and C_2 symmetries, respectively. Single crystals of TBA_6·H_2·**I** suitable for the X-ray structure analysis were successfully obtained and the anion part was a monomeric γ-Keggin divacant silicodecatungstate with two protonated bridging oxygen atoms. Compounds H_3·**I**, H_2·**I**, and H·**I** were reversibly monoprotonated to form H_4·**I**, H_3·**I**, and H_2·**I**, respectively.

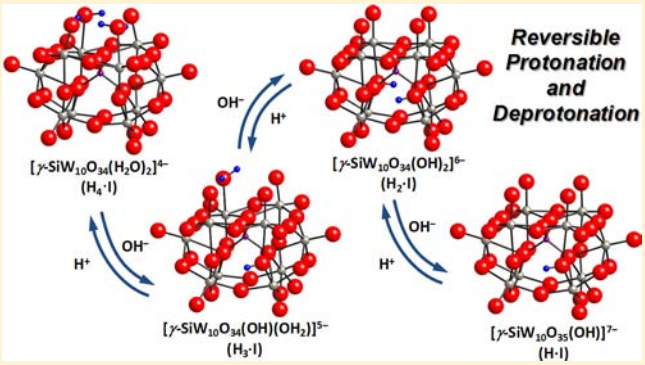

INTRODUCTION

Polyoxometalates (POMs) are a large family of anionic metal–oxygen clusters of early transition metals and have stimulated many current research activities in broad fields such as catalysis, material science, and medicine, because their chemical and physical properties can finely be tuned by choosing constituent elements and counter cations.[1,2] Especially, lacunary POMs are not only important precursors of transition-metal-substituted POMs[1,2] but also important catalysts: Protonation of a γ-Keggin divacant silicodecatungstate, $[\gamma\text{-}SiW_{10}O_{36}]^{8-}$ (**I**), is crucial for H_2O_2-based epoxidation and a tetra-protonated $[\gamma\text{-}SiW_{10}O_{34}(H_2O)_2]^{4-}$ (H_4·**I**) can act as an efficient homogeneous catalyst for H_2O_2-based oxidation of alkenes, allylic alcohols, sulfides, and organosilanes.[3] After the first report on epoxidation of alkenes with H_2O_2, experimental and theoretical studies on H_4·**I** and the related compounds have been reported by several research groups.[4−6]

The structural assignment of the four protons at the lacunary sites has been investigated by density functional theory (DFT) calculations. Bonchio and co-workers have insisted that $[\gamma\text{-}SiW_{10}O_{34}(H_2O)_2]^{4-}$ with two aqua and two oxo groups is energetically favored over $[\gamma\text{-}SiW_{10}O_{32}(OH)_4]^{4-}$ with four hydroxo ligands based on the relativistic DFT calculation including solvent effects,[5] while Musaev and co-workers have reported that $[\gamma\text{-}SiW_{10}O_{32}(OH)_4]^{4-}$ is calculated to be more stable than $[\gamma\text{-}SiW_{10}O_{34}(H_2O)_2]^{4-}$.[4] The NMR spectroscopic studies show that two protons of H_4·**I** are acidic to be abstracted by TBAOH.[5] The resulting tri- and doubly protonated POMs, $[\gamma\text{-}SiW_{10}O_{34}(OH)(OH_2)]^{7-}$ (H_3·**I**) and $[\gamma\text{-}SiW_{10}O_{34}(OH)_2]^{6-}$ (H_2·**I**), have been proposed to possess intramolecular hydrogen bonds between lacunary oxygen atoms, while the bridging oxygen atoms are more favorable monoprotonation sites compared with the terminal and lacunary oxygen atoms on the basis of the calculated molecular electrostatic potential surface of **I**. Therefore, the protonation sites of the doubly protonated POM and reversibility among H_4·**I**, H_3·**I**, H_2·**I**, and a monoprotonated silicodecatungstate (H·**I**) by the deprotonation/protonation are still unclear.

In this paper, we report in situ formation of tri-, doubly-, and monoprotonated silicodecatungstates, $[\gamma\text{-}SiW_{10}O_{34}(OH)(OH_2)]^{5-}$ (H_3·**I**), $[\gamma\text{-}SiW_{10}O_{34}(OH)_2]^{6-}$ (H_2·**I**), and $[\gamma\text{-}SiW_{10}O_{35}(OH)]^{7-}$ (H·**I**), and successful determination of the crystal structure of TBA_6·H_2·**I**. *This study provides the first example of the structurally characterized γ-Keggin divacant POMs with two bridging hydroxo groups.* In addition, the reversible protonation and deprotonation behaviors among H_4·**I**, H_3·**I**, H_2·**I**, and H·**I** are also investigated by potentiometric titrations and NMR spectroscopies.

EXPERIMENTAL SECTION

Materials. Acetonitrile (Kanto Chemical) was purified by The Ultimate Solvent System (GlassContour Company) prior to use.[7] Cyclooctene was purified according to reported procedures.[8] Tetra-*n*-butylammonium bromide (TCI), tetra-*n*-butylammonium hydroxide 30-hydrate (Aldrich), deuterated solvents (deuterium oxide, chloroform-d_1, and dimethyl sulfoxide (DMSO)-d_6) (ACROS), Na_2WO_4·$2H_2O$ (Nippon Inorganic Color & Chemical), Na_2SiO_3·$9H_2O$ (Kanto Chemical), and hydrogen peroxide (30%

Received: May 23, 2012
Published: July 5, 2012

dx.doi.org/10.1021/ic3010773 | Inorg. Chem. 2012, 51, 7932−7939

aqueous solution, Kanto Chemical) were used as received. A divacant silicodecatungstate, $K_8[\gamma\text{-}SiW_{10}O_{36}]\cdot 12H_2O$, was synthesized according to literature procedures.[9]

Instruments. IR spectra were measured on a JASCO FTIR-460 spectrometer using KBr disks. NMR spectra were recorded on a JEOL JNM-EX-270 spectrometer (^{1}H, 270.0 MHz; ^{13}C, 67.80 MHz; ^{29}Si, 53.45 MHz; ^{183}W, 11.20 MHz) by using 5 mm (for ^{1}H and ^{13}C) or 10 mm (for ^{29}Si and ^{183}W) tubes. Chemical shifts (δ) were reported in ppm downfield from $SiMe_4$ (solvent, $CDCl_3$) for ^{1}H, ^{13}C, and ^{29}Si NMR spectra and from 2 M Na_2WO_4 (solvent, D_2O) for ^{183}W NMR spectra. All the NMR measurements were completed within 6 h. GC analyses were performed on Shimadzu GC-2014 with a flame ionization detector equipped with a DB-WAX etr capillary column (internal diameter = 0.25 mm, length = 30 m). Mass spectra were recorded on Shimadzu GCMS-QP2010 equipped with a TC-5HT capillary column at an ionization voltage of 70 eV. Cold-spray ionization mass spectra were measured on a JEOL JMS-T100CS spectrometer in the negative ion mode by direct infusion with a syringe pump (0.05 mL min^{-1}).

Synthesis and Characterization of $[(n\text{-}C_4H_9)_4N]_4[\gamma\text{-}SiW_{10}O_{34}(H_2O)_2]$. A small amount of acetamide was formed during the purification by the precipitation method.[10,11] The ^{1}H and ^{13}C signals of acetamide were not observed for the purified $TBA_4\cdot H_4\cdot$**I** obtained by washing with an excess amount of water. Therefore, the synthetic procedures for $TBA_4\cdot H_4\cdot$**I** were modified, and the purified $TBA_4\cdot H_4\cdot$**I** obtained by washing with an excess amount of water was used throughout the work described in this manuscript. The synthetic procedures for $TBA_4\cdot H_4\cdot$**I** were modified as follows: $K_8[\gamma\text{-}SiW_{10}O_{36}]\cdot 12H_2O$ (6 g, 2 mmol) was dissolved in 60 mL of H_2O, and the pH of this aqueous solution was carefully adjusted to 2.0 with HNO_3. After stirring the solution for 5 min at 293 K, an excess amount of TBABr (6.46 g, 20 mmol) was added in a single step. The resulting white precipitates of $TBA_4\cdot H_4\cdot$**I** were collected by filtration and then washed with an excess amount of H_2O. After drying, the analytically pure $TBA_4\cdot H_4\cdot$**I** was obtained as white powders. Yield 5.2 g (75%). Elemental analysis calcd (%) for $C_{64}H_{148}N_4O_{36}SiW_{10}$ ($[(n\text{-}C_4H_9)_4N]_4[\gamma\text{-}SiW_{10}O_{34}(H_2O)_2]$), C 22.50, H 4.37, N 1.64, Si 0.82, W 53.81; found, C 22.14, H 4.45, N 1.70, Si 0.80, W 53.20. The IR, Raman, UV–vis, NMR (^{29}Si and ^{183}W), and CSI-MS spectra were the same as those of $TBA_4[\gamma\text{-}SiW_{10}O_{34}(H_2O)_2]$ synthesized with the purification by the precipitation method.[3]

Synthesis and Characterization of $[(n\text{-}C_4H_9)_4N]_6[\gamma\text{-}SiW_{10}O_{34}(OH)_2]$. The TBA salt of $H_2\cdot$**I** was synthesized by the reaction of $TBA_4\cdot H_4\cdot$**I** with 2 equiv of $TBAOH\cdot 30H_2O$ followed by addition of an excess amount of diethyl ether. Into acetonitrile (2 mL) containing $TBA_4\cdot H_4\cdot$**I** (0.34 g, 0.10 mmol), $TBAOH\cdot 30H_2O$ (162 mg, 0.20 mmol) was added at 273 K. After stirring the solution for 2 h at 273 K, an excess amount of diethyl ether (60 mL) was added in a single step, and the solution was kept for 1 day at 293 K. The solution was separated by decantation, and the resulting white precipitates of $TBA_6\cdot H_2\cdot$**I** were evacuated at 293 K. After drying, the analytically pure $TBA_6\cdot H_2\cdot$**I** was obtained as white powders. The single crystals suitable for X-ray crystallographic analysis were obtained as follows: $TBA_6\cdot H_2\cdot$**I** (50 mg, 12.8 μmol) was dissolved in acetonitrile (1 mL) and insoluble materials were removed by filtration. The filtrate was kept for 5 days at 293 K with vapor diffusion of diethyl ether, and the colorless crystals of $TBA_6\cdot H_2\cdot$**I** were obtained (40 mg, 80% yield). Yield 0.19 g (48%). ^{1}H NMR (270.0 MHz, DMSO-d_6, 298 K, TMS) δ = 5.06 ppm ($\Delta\nu_{1/2}$ = 1.9 Hz); ^{29}Si NMR (53.45 MHz, DMSO-d_6, 298 K, TMS) δ = −85.4 ($\Delta\nu_{1/2}$ = 3.2 Hz); ^{183}W NMR (11.20 MHz, DMSO-d_6, 298 K, Na_2WO_4) δ = −117.3 ($\Delta\nu_{1/2}$ = 5.9 Hz), −140.0 ($\Delta\nu_{1/2}$ = 4.8 Hz), and −185.1 ($\Delta\nu_{1/2}$ = 5.3 Hz) with an integrated intensity ratio of 4:4:2, respectively; UV–vis (CH_3CN) λ_{max} (ε) 268 nm (19480 mol^{-1} dm^3 cm^{-1}); IR (KBr), 990, 951, 904, 878, 746, 555, 394, 379, 360, 337, 307 cm^{-1}; positive ion MS (CSI, acetone), m/z 2192 ($[(TBA)_8H_2SiW_{10}O_{36}]^{2+}$) and 4142 ($[(TBA)_7H_2SiW_{10}O_{36}]^{+}$); elemental analysis calcd (%) for $C_{96}H_{218}N_6O_{36}SiW_{10}$ ($[(n\text{-}C_4H_9)_4N]_6[\gamma\text{-}SiW_{10}O_{34}(OH)_2]$), C 29.57, H 5.64, N 2.16, Si 0.72, W 47.15; found, C 29.39, H 5.84, N 2.38, Si 0.72, W 46.79.

X-ray Crystallography. X-ray diffraction measurements were made on a Rigaku AFC-10 Saturn 724 CCD detector with graphite monochromated Mo Kα radiation (λ = 0.71069 Å). The data of $TBA_6\cdot H_2\cdot$**I** were collected using CrystalClear[12] at 153 K, and indexing, integration, and absorption correction were performed with HKL2000[13] software for Linux. Neutral scattering factors were obtained from the standard source. In the data reduction, corrections for Lorentz and polarization effects were made. The structural analysis was performed using CrystalStructure[14] and Win-GX for Windows software.[15] The molecular structure of $TBA_6\cdot H_2\cdot$**I** was solved by combination of SHELXS-97 (direct methods) and SHELXH-97 (Fourier and least-squares refinement).[16] Tungsten, silicon, and oxygen atoms were refined anisotropically, and carbon and nitrogen atoms were refined isotropically. The highly disordered solvent of crystallization (acetonitrile) was omitted by use of SQUEEZE program.[17]

Quantum Chemical Calculations. The calculations were carried out at the B3LYP level theory[18] with 6-31++G** basis sets for H and O atoms, 6-31G** basis sets for Si atom, and the double-ξ quality basis sets with effective core potentials proposed by Hay and Wadt[19] for W atom by using conductor-like polarizable continuum model (CPCM)[20] with the parameters of the United Atom Topological Model (UAHF). The entire structures of mono-, doubly-, and triprotonated γ-Keggin lacunary POMs were used as models, and the geometries were optimized without the symmetry restrictions. The optimized geometries are shown in Supporting Information, Table S1. All calculations were performed with the Gaussian09 program package.[21]

Catalytic Epoxidation of Cyclooctene with Hydrogen Peroxide Catalyzed by $TBA_6\cdot H_2\cdot$I. Catalytic epoxidation was carried out with a glass tube (30 mL) containing a magnetic stir bar. $TBA_6\cdot H_2\cdot$**I** (8 μmol), acetonitrile (6 mL), and cyclooctene (5 mmol) were charged in the reaction vessel. Reaction was initiated by addition of 30% aqueous H_2O_2 (1 mmol). The reaction solution was periodically analyzed by GC. The epoxide yield was determined based on the amount of initial H_2O_2.

RESULTS AND DISCUSSION

NMR Studies on in Situ Formation of $H_3\cdot$I, $H_2\cdot$I, and H·I. The potentiometric titration of $TBA_4\cdot H_4\cdot$**I** with TBAOH is shown in Figure 1a. The electric potential gradually decreased upon addition of TBAOH, and inflection points at 2 and 3 equiv of TBAOH with respect to $TBA_4\cdot H_4\cdot$**I** were observed. The in situ formation of $H_2\cdot$**I** and H·**I** could be confirmed by the ^{1}H, ^{29}Si, and ^{183}W NMR spectroscopies in DMSO-d_6 as follows: Upon addition of 2 equiv of TBAOH with respect to $TBA_4\cdot H_4\cdot$**I**, the ^{183}W NMR spectrum showed 3 signals at −122.9, −156.8, and −191.7 ppm with the respective intensity ratio of 2:2:1 and the signals of $H_4\cdot$**I** disappeared (Supporting Information, Figure S1 and entry 5 in Table 1), in accord with the ^{183}W NMR results reported by Bonchio and coworkers.[5] The ^{183}W signals of in situ formed $H_2\cdot$**I** were not changed after the solution was kept at 298 K for 48 h, showing that $H_2\cdot$**I** is stable. Upon further addition of 1 equiv (the sum total; 3 equiv) of TBAOH with respect to $TBA_4\cdot H_4\cdot$**I**, a new strong ^{1}H signal appeared at 6.43 ppm, and the intensity of the 5.00-ppm signal of $H_2\cdot$**I** much decreased (Figure 2c and entry 7 in Table 1). In addition, the ^{183}W NMR spectrum showed new five strong signals at −81.3, −129.3, −155.1, −157.9, and −174.1 ppm with the respective intensity ratio of 1:1:1:1:1 and the intensities of the −122.9, −156.8, and −191.7-ppm signals of $H_2\cdot$**I** much decreased (Figure 2b). In the same way, a new strong ^{29}Si signal appeared at −86.1 ppm and the intensity of the −85.4-ppm signal of $H_2\cdot$**I** much decreased (Figure 2a). All these ^{1}H, ^{29}Si, and ^{183}W NMR data suggest the formation of a monoprotonated species with C_2 symmetry. Upon further

dx.doi.org/10.1021/ic3010773 | Inorg. Chem. 2012, 51, 7932–7939

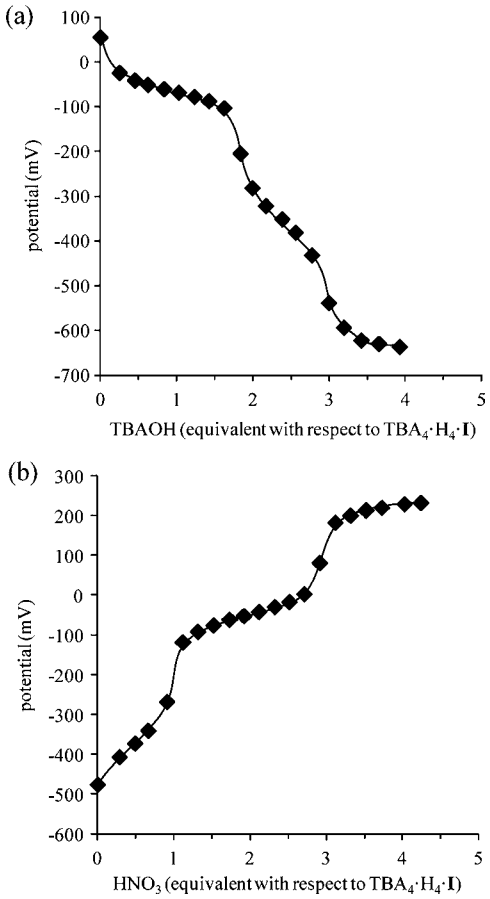

Figure 1. Profiles for the potentiometric titration of (a) $TBA_4{\cdot}H_4{\cdot}\mathbf{I}$ (0.01 M) in a mixed solvent of DMSO and water (9/1, v/v) with 1 M aqueous TBAOH as a titrant and (b) $TBA_7{\cdot}H{\cdot}\mathbf{I}$ (0.01 M, in situ formed by the reaction of $TBA_4{\cdot}H_4{\cdot}\mathbf{I}$ with 3 equiv of TBAOH) in a mixed solvent of DMSO and water (9/1, v/v) with 1 M aqueous HNO_3 as a titrant. The potentials are relative to a standard Ag/AgCl electrode.

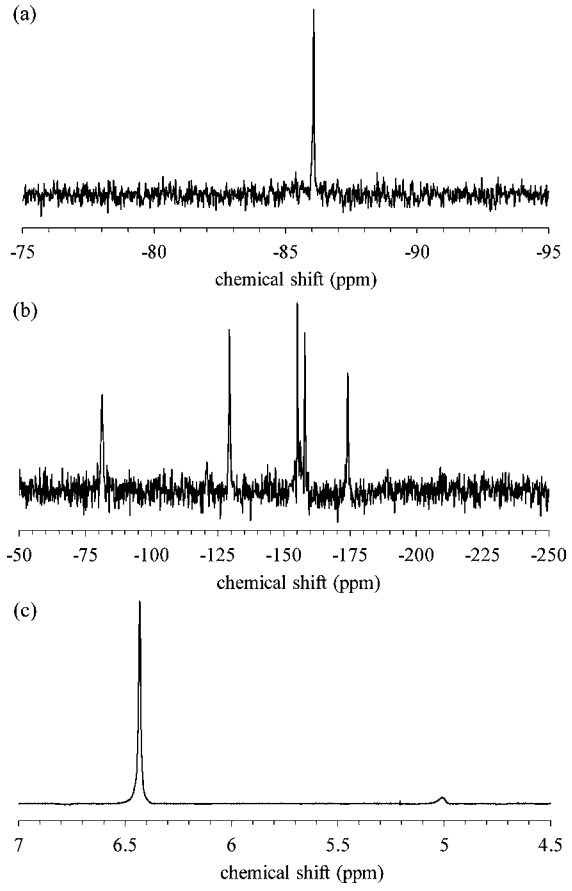

Figure 2. (a) ^{29}Si, (b) ^{183}W, and (c) ^{1}H NMR spectra of $TBA_4{\cdot}H_4{\cdot}\mathbf{I}$ upon addition of 3 equiv of TBAOH (solvent, DMSO-d_6; 298 K; (a) $[TBA_4{\cdot}H_4{\cdot}\mathbf{I}]$ = 0.16 M, 2359 scans; (b) $[TBA_4{\cdot}H_4{\cdot}\mathbf{I}]$ = 0.16 M, 20918 scans; (c) $[TBA_4{\cdot}H_4{\cdot}\mathbf{I}]$ = 0.10 M, 128 scans).

addition of 1 equiv (the sum total; four equivalents) of TBAOH with respect to $TBA_4{\cdot}H_4{\cdot}\mathbf{I}$, only ^{29}Si and ^{183}W signals assignable to $H{\cdot}\mathbf{I}$ were still observed within 6 h. These NMR spectroscopies show that three protons of $H_4{\cdot}\mathbf{I}$ are acidic to be abstracted by TBAOH in accord with the stability of $[\gamma\text{-}HSiW_{10}O_{36}]^{7-}$ in aqueous solution.[9a]

The solution-states during the reaction of $TBA_4{\cdot}H_4{\cdot}\mathbf{I}$ with less than 2 equiv of TBAOH were investigated (Supporting Information, Figures S1 and S2). Upon addition of 1 equiv of TBAOH with respect to $TBA_4{\cdot}H_4{\cdot}\mathbf{I}$, a new strong ^{1}H signal appeared at 4.74 ppm with the integrated signal intensity of one equivalent proton with respect to **I**. The ^{1}H signals of the aqua ligands in $H_4{\cdot}\mathbf{I}$ were not observed probably because of the ligand exchange of the aqua ligands with DMSO.[10,11] Therefore, the appearance of one equivalent proton suggests that $H_3{\cdot}\mathbf{I}$ possesses one aqua and one hydroxo groups. In addition, a new strong ^{29}Si signal appeared at −84.4 ppm with the weak signals of $H_2{\cdot}\mathbf{I}$ and $H_4{\cdot}\mathbf{I}$. In the same way, the ^{183}W NMR spectrum showed 10 strong signals at −78.0, −98.0, −98.9, −131.8, −133.3, −146.4, −158.2, −160.8, −183.0, and −197.6 ppm with the respective intensity ratio of 1:1:1:1:1:1:1:1:1:1 in addition to the weak signals of $H_2{\cdot}\mathbf{I}$ and $H_4{\cdot}\mathbf{I}$. All these ^{1}H, ^{29}Si, and ^{183}W NMR data suggest the

Table 1. NMR Parameters of $TBA_4{\cdot}H_4{\cdot}\mathbf{I}$ and $TBA_6{\cdot}H_2{\cdot}\mathbf{I}$ and in Situ Formed $H_4{\cdot}\mathbf{I}$, $H_3{\cdot}\mathbf{I}$, $H_2{\cdot}\mathbf{I}$, and $H{\cdot}\mathbf{I}$

		chemical shift (ppm)		
entry	compound	^{1}H	^{29}Si	^{183}W
1	$TBA_4{\cdot}H_4{\cdot}\mathbf{I}$	not observed	−83.2	−95.2, −98.2, −116.8, −118.2, −194.3
2	$TBA_6{\cdot}H_2{\cdot}\mathbf{I}$	5.06	−85.4	−117.3, −140.0, −185.1
3	in situ formed $H_4{\cdot}\mathbf{I}$ ($TBA_6{\cdot}H_2{\cdot}\mathbf{I}$ + 2 equiv. HNO_3)	not observed	−83.4	−98.5, −100.3, −114.0, −121.3, −184.0
4	in situ formed $H_3{\cdot}\mathbf{I}$ ($TBA_4{\cdot}H_4{\cdot}\mathbf{I}$ + 1 equiv. TBAOH)	4.74	−84.4	−78.0, −98.0, −98.9, −131.8, −133.3, −146.4, −158.2, −160.8, −183.0, −197.6
5	in situ formed $H_2{\cdot}\mathbf{I}$ ($TBA_4{\cdot}H_4{\cdot}\mathbf{I}$ + 2 equiv. TBAOH)	5.00	−85.4	−122.9, −156.8, −191.7
6	in situ formed $H_2{\cdot}\mathbf{I}$ (in situ formed $H{\cdot}\mathbf{I}$ + 1 equiv. HNO_3)	5.01	−85.4	−122.0, −157.7, −190.1
7	in situ formed $H{\cdot}\mathbf{I}$ ($TBA_4{\cdot}H_4{\cdot}\mathbf{I}$ + 3 equiv. TBAOH)	6.43	−86.1	−81.3, −129.3, −155.1, −157.9, −174.1

dx.doi.org/10.1021/ic3010773 | Inorg. Chem. 2012, 51, 7932−7939

formation of a nonsymmetric triprotonated species, [γ-$SiW_{10}O_{34}(H_2O)(OH)]^{5-}$ (H_3·**I**).

Distributions of H_4·**I**, H_3·**I**, and H_2·**I** against the amounts of TBAOH added are shown in Figure 3.[22] The fraction of H_4·**I**

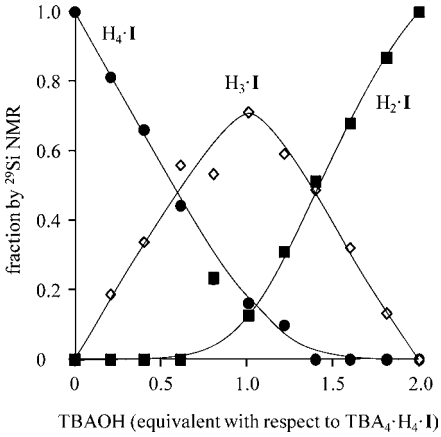

Figure 3. Distributions of H_4·**I**, H_3·**I**, and H_2·**I** against the amounts of TBAOH added (solvent, DMSO-d_6; 298 K; [TBA_4·H_4·**I**] = 0.16 M). The fractions of H_4·**I**, H_3·**I**, and H_2·**I** were determined by the ^{29}Si NMR data.

decreased followed by increase in the fraction of H_3·**I**, which reached a maximum at 1 equiv of TBAOH. The fractions of H_4·**I** and H_3·**I** completely disappeared at 2 equiv of TBAOH. The fraction of H_2·**I** started to increase after addition of about 0.6 equiv of TBAOH and reached 1.0 at 2 equiv of TBAOH. These results suggest a consecutive reaction of H_4·**I** → H_3·**I** → H_2·**I**.[23]

Synthesis and Structural Characterization of TBA_6·H_2·I. Isolation of doubly- and monoprotonated silicodecatungstates (H_2·**I** and H·**I**) was attempted by the reaction of TBA_4·H_4·**I** with 2 and 3 equiv of TBAOH, respectively, followed by addition of an excess amount of diethyl ether. Single crystals of TBA_6·H_2·**I** suitable for the X-ray structure analysis were successfully obtained by recrystallization from acetonitrile solution of H_2·**I** with vapor diffusion of diethyl ether,[24] while the isolation of H·**I** was unsuccessful.[25] Ball and stick and polyhedral representations of the anion part of TBA_6·H_2·**I** are shown in Figure 4. POM H_2·**I** is a monomeric γ-Keggin divacant silicodecatungstate. The existence of six TBA cations per the anion of H_2·**I** implies that the charge of the anion is −6. The elemental analysis data revealed that the molar ratio of TBA:Si:W was 6:1:10, respectively, in accord with the crystallographic data. Selected bond lengths and angles for H_2·**I** are shown in Table 2. While four tungsten atoms (W1, W2, W3, and W4) at the lacunary sites have two terminal oxygen atoms, the other six tungsten atoms (W5, W6, W7, W8, W9, and W10) have one terminal oxygen atom. The terminal W−O bond lengths at the lacunary sites of H_2·**I** (1.72−1.76 Å) were close to each other, while two of eight W−O bonds at the lacunary sites of [γ-$SiW_{10}O_{34}(H_2O)_2]^{4-}$ are long (2.14 and 2.16 Å vs 1.70−1.75 Å).[3a] The bond valence sum (BVS) values of tungsten (5.80−6.16) and silicon (3.81) indicate that respective valences are +6 and +4. The BVS values of O20 (1.16) and O25 (1.16) were lower than those of the other oxygen atoms (1.55−2.10) (Supporting Information, Table S2). These results indicate that O20 and O25 are monoprotonated, resulting in μ-OH groups. *To date, lacunary POMs with hydroxo group(s) have not yet experimentally been synthesized and structurally characterized.*[3,26]

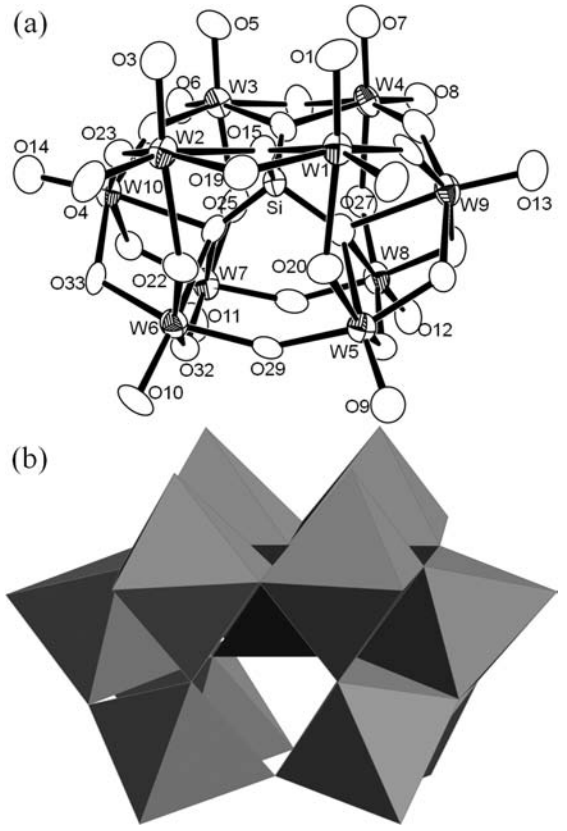

Figure 4. (a) Ball and stick and (b) polyhedral representations of the anion part of TBA_6·H_2·**I**. Thermal ellipsoid set at 50% probability. Gray and purple polyhedra show the [WO_6] and [SiO_4] units, respectively.

The ^{183}W NMR spectrum of TBA_6·H_2·**I** in DMSO-d_6 were identical to those of the in situ formed H_2·**I** (entry 2 in Table 1): Three signals at −117.3, −140.0, and −185.1 ppm with the respective intensity ratio of 2:2:1 were observed (Figure 5b).[27] The ^{183}W signals of TBA_6·H_2·**I** appeared at lower fields than those of the in situ formed H_2·**I** (TBA_4·H_4·**I** with 2 equiv of TBAOH). Upon addition of 62 equiv of water (i.e., the amount of water in the reaction solution of TBA_4·H_4·**I** with 2 equiv of TBAOH·30H_2O) to the solution of TBA_6·H_2·**I**, three ^{183}W signals were observed at −121.2, −155.3, and −189.9 ppm with the respective intensity ratio of 2:2:1, and the chemical shifts were almost the same as those of in situ formed H_2·**I**. Therefore, the upfield shifts of the ^{183}W signals of the in situ formed H_2·**I** would result from the presence of water. The ^{29}Si NMR spectrum of TBA_6·H_2·**I** in DMSO-d_6 showed one signal at −85.4 ppm (Figure 5a). The ^{1}H NMR spectrum of TBA_6·H_2·**I** in DMSO-d_6 showed one signal at 5.06 ppm assignable to the hydroxo protons (Figure 5c). The positive-ion CSI-MS spectrum of TBA_6·H_2·**I** in acetone showed the most intense peaks (centered at m/z = 2192 and 4142) with isotopic distributions that agree with the patterns calculated for $TBA_8[H_2SiW_{10}O_{36}]^{2+}$ and $TBA_7[H_2SiW_{10}O_{36}]^{+}$, respectively (Figure 6). All these NMR and CSI-MS results suggest that the anion part of TBA_6·H_2·**I** is a single doubly protonated species with the C_{2v} symmetry in DMSO and that the solid-state structure is maintained in the solution-state.

dx.doi.org/10.1021/ic3010773 | *Inorg. Chem.* 2012, 51, 7932−7939

Table 2. Experimental and Calculated Selected Bond Lengths (in Å) and Angles (in degree) of [γ-$SiW_{10}O_{34}(OH)_2$]$^{6-}$

		calculated H_2·**I** doubly protonated at	
	experimental (TBA_6·H_2·**I**)	O20 and O25	O1 and O5
W1−O1	1.726(15)	1.746	1.950
W1−O2	1.755(13)	1.749	1.733
W2−O3	1.716(16)	1.748	1.748
W2−O4	1.743(14)	1.748	1.752
W3−O5	1.736(15)	1.746	1.950
W3−O6	1.755(15)	1.749	1.732
W4−O7	1.746(16)	1.748	1.748
W4−O8	1.745(15)	1.748	1.752
W5−O9	1.738(17)	1.734	1.738
W6−O10	1.742(13)	1.740	1.741
W7−O11	1.722(14)	1.734	1.738
W8−O12	1.724(15)	1.740	1.741
W9−O13	1.736(15)	1.735	1.737
W10−O14	1.732(15)	1.735	1.737
W1−O20	2.308(13)	2.377	1.911
W2−O22	2.240(12)	2.277	2.276
W3−O25	2.311(15)	2.377	1.911
W4−O27	2.240(14)	2.277	2.276
W1−O20−W5	136.3(7)	138.38	147.77
W2−O22−W6	139.4(6)	144.45	140.51
W3−O25−W7	137.0(7)	138.38	147.77
W4−O27−W8	141.4(7)	144.45	140.51

To compare the catalytic activity of TBA_6·H_2·**I** with that of TBA_4·H_4·**I**, epoxidation of cyclooctene with H_2O_2 was carried out. The TBA_6·H_2·**I**-catalyzed epoxidation gave 1,2-epoxycyclooctane in 15% yield for 2 h. Yield of TBA_6·H_2·**I** was much lower than that (>99%) of TBA_4·H_4·**I**, showing that the tetraprotonation of **I** is crucial for the present epoxidation.

DFT Calculations on the Structures of H_3·I**, H_2·**I**, and H·**I**.** To investigate the protonation sites in more detail, the DFT calculations were carried out taking into account the solvation in DMSO using the conductor-like polarizable continuum model (CPCM) with the parameters of the United Atom Topological Model (UAHF). The structures of doubly protonated [γ-$SiW_{10}O_{34}(OH)_2$]$^{6-}$ were optimized (Figures 7a and 7b). POM H_2·**I** doubly protonated at O20 and O25 was calculated to be more stable than that at O1 and O5 by 13 kJ mol^{-1}. In addition, the calculated geometry of POM H_2·**I** doubly protonated at O20 and O25 agreed well with experimental one (Table 2). These results support that O20 and O25 are protonated. In addition, the dynamic behavior of H_2·**I** was investigated by the variable temperature ^{29}Si NMR experiments (233−333 K). The ^{29}Si NMR spectrum of isolated TBA_6·H_2·**I** in acetonitrile-d_3 at 233 K showed one signal at −85.6 ppm ($\Delta\nu_{1/2}$ = 1.2 Hz). The signal slightly shifted to downfield with increase in the temperature (−85.5 ($\Delta\nu_{1/2}$ = 1.2 Hz) at 293 K and −85.3 ppm ($\Delta\nu_{1/2}$ = 1.3 Hz) at 333 K) and no new signal appeared. The slight shift is in accord with the result that the H_2·**I** doubly protonated at O20 and O25 is calculated to be more stable by 13 kJ mol^{-1} than that at O1 and O5.

The monoprotonation sites of **I** were also investigated taking into account the hydrogen bonds between adjacent oxygen atoms. The structures of monoprotonated [γ-Si-$W_{10}O_{35}(OH)$]$^{7-}$ were optimized, and the relative energies were compared (Figure 8). POM H·**I** protonated at O20 (**H**) was calculated to be more stable than those (**A**−**G** and **I**−**K**) of the others by 3−77 kJ mol^{-1}, showing that O20 is the most

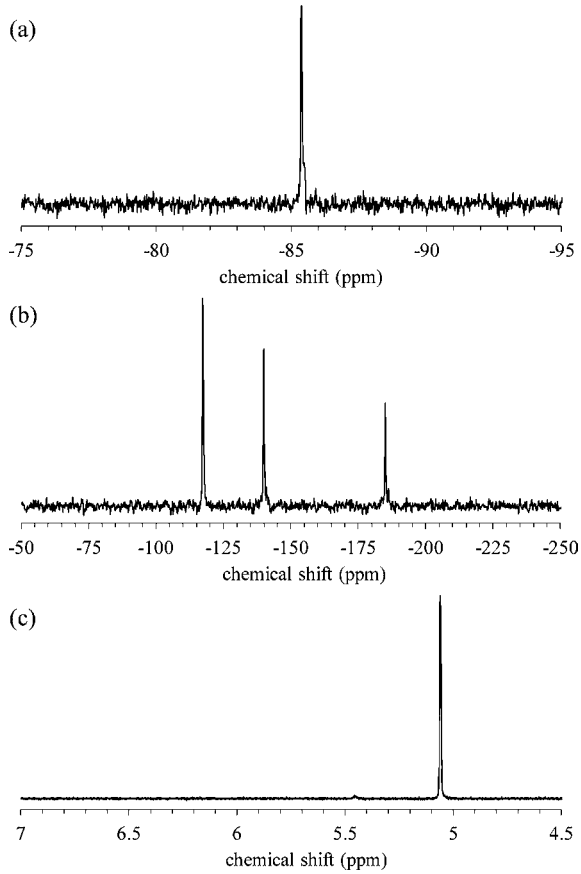

Figure 5. (a) ^{29}Si, (b) ^{183}W, and (c) ^{1}H NMR spectra of TBA_6·H_2·**I** (solvent, DMSO-d_6; 298 K; (a) [TBA_6·H_2·**I**] = 0.18 M, 2048 scans; (b) [TBA_6·H_2·**I**] = 0.18 M, 9758 scans; (c) [TBA_6·H_2·**I**] = 0.16 M, 32 scans).

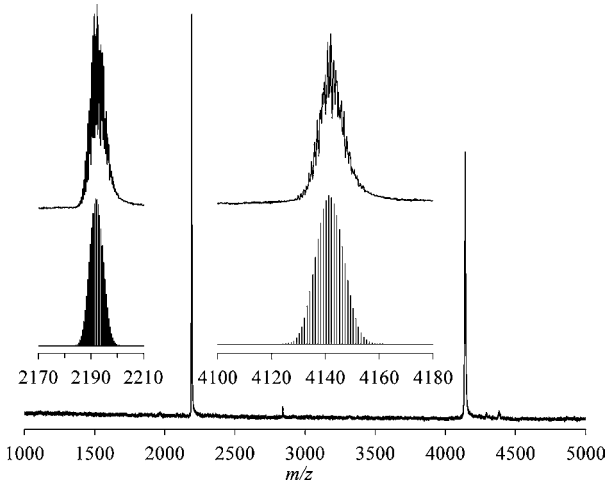

Figure 6. Positive-ion CSI-MS spectra (m/z = 1000−5000) of TBA_6·H_2·**I** (Solvent:acetone). Inset: CSI-MS spectra (m/z = 2170−2210 and 4100−4180) of TBA_6·H_2·**I** and calculated patterns of $TBA_8[H_2SiW_{10}O_{36}]^{2+}$ (m/z = 2192) and $TBA_7[H_2SiW_{10}O_{36}]^{+}$ (m/z = 4142).

dx.doi.org/10.1021/ic3010773 | Inorg. Chem. 2012, 51, 7932−7939

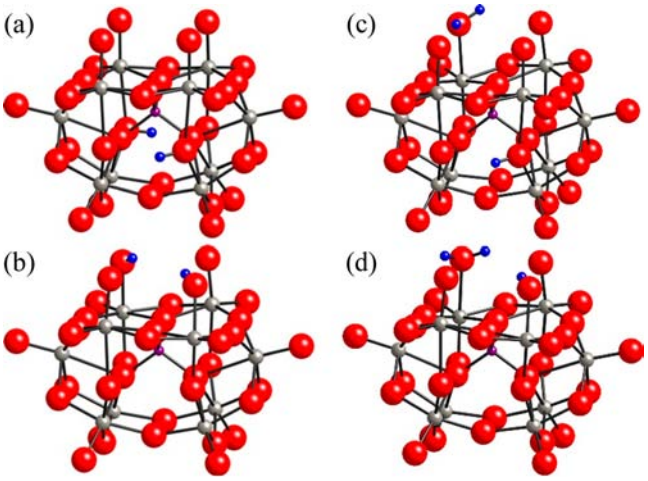

Figure 7. Ball and stick representations for calculated structures of POM H_2·**I** doubly protonated at (a) O20 and O25 and (b) O1 and O5 and POM H_3·**I** (c) doubly protonated at O5 and monoprotonated at O20 and (d) doubly protonated at O5 and monoprotonated at O1. Gray, red, purple, and blue balls represent tungsten, oxygen, silicon, and hydrogen atoms, respectively.

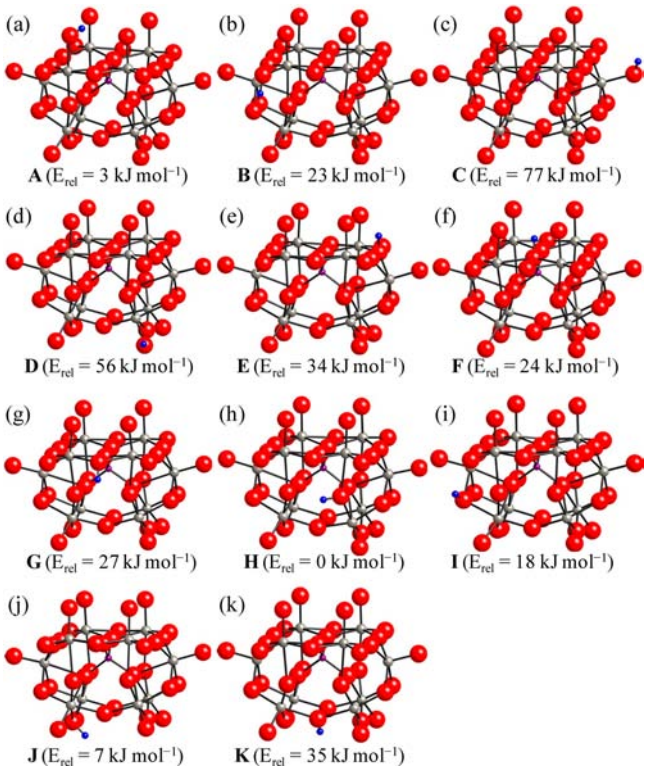

Figure 8. Ball and stick representations for calculated structures of monoprotonated $[\gamma\text{-}SiW_{10}O_{35}(OH)]^{7-}$ (**A**–**K**) and relative energies with respect to **H**. Gray, red, purple, and blue balls represent tungsten, oxygen, silicon, and hydrogen atoms, respectively.

favorable monoprotonation site. Similarly, the structures of triprotonated $[\gamma\text{-}SiW_{10}O_{34}(H_2O)(OH)]^{5-}$ were optimized (Figures 7c and 7d). POM H_3·**I** doubly protonated at O5 and monoprotonated at O20 was calculated to be more stable by 9 kJ·mol^{-1} than that doubly protonated at O5 and monoprotonated at O1, suggesting that O5 and O20 are more favorable protonation sites than O5 and O1.

Reversible Protonation and Deprotonation Behaviors. The potentiometric titration of a monoprotonated H·**I**, which was in situ formed by the reaction of TBA_4·H_4·**I** with 3 equiv of TBAOH, with HNO_3 showed inflection points at 1 and 3 equiv of HNO_3 with respect to H·**I** (Figure 1b). Upon addition of 1 equiv of HNO_3 with respect to H·**I**, the 5.01-ppm ^{1}H signal of H_2·**I** appeared again (entry 6 in Table 1). The ^{29}Si NMR spectrum showed one signal at −85.4 ppm and the ^{183}W NMR spectrum exhibited three signals at −122.0, −157.7, and −190.1 ppm with the respective intensity ratio of 2:2:1 (Supporting Information, Figure S4). Similarly, the potentiometric titration of TBA_6·H_2·**I** with HNO_3 showed an inflection point at 2 equiv of protons with respect to TBA_6·H_2·**I** (Supporting Information, Figure S5). Upon addition of 2 equiv of HNO_3 with respect to TBA_6·H_2·**I**, the ^{1}H NMR signal assignable to a hydroxo proton disappeared (Supporting Information, Figure S6 and entry 3 in Table 1). The ^{29}Si NMR spectrum showed one signal at −83.4 ppm and the ^{183}W NMR spectrum exhibited five signals at −98.5, −100.3, −114.0, −121.3, and −184.0 ppm with the respective intensity ratio of 1:1:1:1:1. The formation of H_3·**I** by the reaction of in situ formed H_2·**I** with 1 equiv of TBAOH was also confirmed by ^{1}H NMR spectroscopy. All these results suggest that H·**I**, H_2·**I**, and H_3·**I** react with one proton to form doubly-, tri-, and tetraprotonated H_2·**I**, H_3·**I**, and H_4·**I**, respectively, and that these reactions are reversible (eq 1).

$$[\gamma\text{-}SiW_{10}O_{34}(H_2O)_2]^{4-} \underset{H^+}{\overset{OH^-}{\rightleftharpoons}} [\gamma\text{-}SiW_{10}O_{34}(OH)(OH_2)]^{5-} \underset{H^+}{\overset{OH^-}{\rightleftharpoons}} [\gamma\text{-}SiW_{10}O_{34}(OH)_2]^{6-} \underset{H^+}{\overset{OH^-}{\rightleftharpoons}} [\gamma\text{-}SiW_{10}O_{35}(OH)]^{7-} \quad (1)$$

(H_4·**I**) (H_3·**I**) (H_2·**I**) (H·**I**) (in DMSO)

CONCLUSIONS

In conclusion, we investigated the reversible protonation and deprotonation behaviors among H_4·**I**, H_3·**I**, H_2·**I**, and H·**I** by the potentiometric titrations and NMR (^{1}H, ^{29}Si, and ^{183}W) spectroscopies. By the reaction of H_4·**I** with 1, 2, and 3 equiv of TBAOH, H_3·**I**, H_2·**I**, and H·**I** with C_1, C_{2v}, and C_2 symmetries, respectively, were formed in situ. A doubly protonated POM TBA_6·H_2·**I** was successfully synthesized, and the X-ray crystallographic analysis showed that the anion part was a monomeric γ-Keggin divacant silicodecatungstate with two protonated bridging oxygen atoms. This is the first example of the structurally characterized γ-Keggin divacant POMs with two bridging hydroxo groups. Compounds H_3·**I**, H_2·**I**, and H·**I** were reversibly monoprotonated to form H_4·**I**, H_3·**I**, and H_2·**I**, respectively.

ASSOCIATED CONTENT

Supporting Information

Crystallographic data in CIF format, Cartesian coordinates of the calculated structures, BVS calculations, profile for potentiometric titration, NMR spectra, and the complete citation of ref 21. This material is available free of charge via the Internet at http://pubs.acs.org.

AUTHOR INFORMATION

Corresponding Author

*E-mail: tmizuno@mail.ecc.u-tokyo.ac.jp.

dx.doi.org/10.1021/ic3010773 | *Inorg. Chem.* 2012, 51, 7932–7939

Notes

The authors declare no competing financial interest.

■ ACKNOWLEDGMENTS

This work was supported in part by the Japan Society for the Promotion of Science (JSPS) through its "Funding Program for World-Leading Innovative R&D on Science and Technology (FIRST Program)" and a Grant-in-Aid for Scientific Research from the Ministry of Education, Culture, Science, Sports, and Technology of Japan.

■ REFERENCES

(1) (a) Pope, M. T. *Heteropoly and Isopoly Oxometalates*; Springer-Verlag: Berlin, Germany, 1983. (b) Thematic issue on "Polyoxometalates", *Chem. Rev.* **1998**, *98*, 1−389. (c) Pope, M. T. In *Comprehensive Coordination Chemistry II*; McCleverty, J. A., Meyer, T. J., Eds.; Elsevier Pergamon: Amsterdam, The Netherlands, 2004; Vol. 4, pp 635−678. (d) Mialane, P.; Dolbecq, A.; Sécheresse, F. *Chem. Commun.* **2006**, 3477−3485. (e) Proust, A.; Thouvenot, R.; Gouzerh, P. *Chem. Commun.* **2008**, 1837−1852. (f) Kögerler, P.; Tsukerblat, B.; Müller, A. *Dalton Trans.* **2010**, *39*, 21−36. (g) Long, D.-L.; Tsunashima, R.; Cronin, L. *Angew. Chem., Int. Ed.* **2010**, *49*, 1736−1758. (h) Bassil, B. S.; Kortz, U. *Dalton Trans.* **2011**, *40*, 9649−9661.

(2) (a) Hill, C. L.; Chrisina, C.; Prosser-McCartha, M. *Coord. Chem. Rev.* **1995**, *143*, 407−455. (b) Okuhara, T.; Mizuno, N.; Misono, M. *Adv. Catal.* **1996**, *41*, 113−252. (c) Kozhevnikov, I. V. *Catalysts for Fine Chemical Synthesis, Vol. 2, Catalysis by Polyoxometalates*, John Wiley & Sons: Chichester, U.K., 2002. (d) Hill, C. L. In *Comprehensive Coordination Chemistry II*; *Vol. 4*; McCleverty, J. A., Meyer, T. J., Eds.; Elsevier Science: New York, 2004; pp 679−759. (e) Neumann, R.; Khenkin, A. M. *Chem. Commun.* **2006**, 2529−2538. (f) Mizuno, N.; Kamata, K.; Uchida, S.; Yamaguchi, K. In *Modern Heterogeneous Oxidation Catalysis*; Mizuno, N., Ed.; Wiley-VCH: Weinheim, Germany, 2009; pp185−216.

(3) (a) Kamata, K.; Yonehara, K.; Sumida, Y.; Yamaguchi, K.; Hikichi, S.; Mizuno, N. *Science* **2003**, *300*, 964−966. (b) Kamata, K.; Nakagawa, Y.; Yamaguchi, K.; Mizuno, N. *J. Catal.* **2004**, *224*, 224−228. (c) Mizuno, N.; Yamaguchi, K.; Kamata, K. *Coord. Chem. Rev.* **2005**, *249*, 1944−1956. (d) Kamata, K.; Kotani, M.; Yamaguchi, K.; Hikichi, S.; Mizuno, N. *Chem.—Eur. J.* **2007**, *13*, 639−648. (e) Ishimoto, R.; Kamata, K.; Mizuno, N. *Angew. Chem., Int. Ed.* **2009**, *48*, 8900−8904.

(4) (a) Musaev, D. G.; Morokuma, K.; Geletii, Y. V.; Hill, C. L. *Inorg. Chem.* **2004**, *43*, 7702−7708. (b) Prabhakar, R.; Morokuma, K.; Hill, C. L.; Musaev, D. G. *Inorg. Chem.* **2006**, *45*, 5703−5709.

(5) (a) Sartorel, A.; Carraro, M.; Bagno, A.; Scorrano, G.; Bonchio, M. *Angew. Chem., Int. Ed.* **2007**, *46*, 3255−3258. (b) Sartorel, A.; Carraro, M.; Bagno, A.; Scorrano, G.; Bonchio, M. *J. Phys. Org. Chem.* **2008**, *21*, 596−602.

(6) (a) Bonchio, M.; Carraro, M.; Scorrano, G.; Bagno, A. *Adv. Synth. Catal.* **2004**, *346*, 648−654. (b) Phan, T. D.; Kinch, M. A.; Barker, J. E.; Ren, T. *Tetrahedron Lett.* **2005**, *46*, 397−400. (c) Carraro, M.; Sandei, L.; Sartorel, A.; Scorrano, G.; Bonchio, M. *Org. Lett.* **2006**, *8*, 3671−3674. (d) Yoshida, A.; Yoshimura, M.; Uehara, K.; Hikichi, S.; Mizuno, N. *Angew. Chem., Int. Ed.* **2006**, *45*, 1956−1960. (e) Yoshida, A.; Hikichi, S.; Mizuno, N. *J. Organomet. Chem.* **2007**, *692*, 455−459. (f) Berardi, S.; Bonchio, M.; Carraro, M.; Conte, V.; Sartorel, A.; Scorrano, G. *J. Org. Chem.* **2007**, *72*, 8954−8957. (g) Carraro, M.; Modugno, G.; Sartorel, A.; Scorrano, G.; Bonchio, M. *Eur. J. Inorg. Chem.* **2009**, 5164−5174. (h) Yoshida, A.; Nakagawa, Y.; Uehara, K.; Hikichi, S.; Mizuno, N. *Angew. Chem., Int. Ed.* **2009**, *48*, 7055−7058.

(7) Pangborn, A. B.; Giardello, M. A.; Grubbs, R. H.; Rosen, R. K.; Timmers, F. J. *Organometallics* **1996**, *15*, 1518−1520.

(8) Perrin, D. D.; Armarego, W. L. F. *Purification of Laboratory Chemicals*, 3rd ed.; Pergamon Press: Oxford, U.K., 1988.

(9) (a) Canny, J.; Tézé, A.; Thouvenot, R.; Hervé, G. *Inorg. Chem.* **1986**, *25*, 2114−2119. (b) Tézé, A.; Hervé, G. *Inorg. Synth.* **1986**, *27*, 85−96.

(10) The ^{1}H NMR spectrum of $TBA_4{\cdot}H_4{\cdot}\mathbf{I}$ in anhydrous DMSO-d_6 showed the signal of water at 3.36 ppm (approximately 2 equiv with respect to $TBA_4{\cdot}H_4{\cdot}\mathbf{I}$) in addition to the 3.18, 2.95, 1.56, and 1.35-ppm signals of TBA. The CSI-MS spectrum of $TBA_4{\cdot}H_4{\cdot}\mathbf{I}$ in DMSO showed two main peaks at m/z = 2011 and 3779 assignable to $TBA_6[SiW_{10}O_{34}(DMSO)_2]^{2+}$ and $TBA_5[SiW_{10}O_{34}(DMSO)_2]^{+}$, respectively. These results suggest the ligand exchange of aqua ligands with DMSO.[11] It has been reported that the ^{1}H NMR spectrum of $TBA_4{\cdot}H_4{\cdot}\mathbf{I}$ in DMSO-d_6 shows two signals at 7.36 and 6.72 ppm assignable to nonequivalent protons.[5] These signals are possibly assignable to those of acetamide (CH_3CONH_2), which would be formed during the purification (precipitation process) of crude $TBA_4{\cdot}H_4{\cdot}\mathbf{I}$. This idea is supported by the following results: (i) The ^{13}C signal at 171.9 ppm assignable to the carbon of acetamide, and (ii) the low integrated intensity of the signals at 7.36 and 6.72 ppm (0.01 equiv of acetamide with respect to TBA).

(11) The coordination of DMSO to tungsten atoms in $[Sb_2W_{20}(OH)_2(DMSO)_2O_{66}]^{8-}$ and $[X_2W_{22}(DMSO)_4O_{72}]^{6-}$ (X = Sb, Bi) has been reported: (a) Bi, L.-H.; Li, B.; Wu, L.-X. *Inorg. Chem. Commun.* **2008**, *11*, 1184−1186. (b) Bi, L.-H.; Hou, G.-F.; Bao, Y.-Y.; Li, B.; Wu, L.-X.; Gao, Z.-M.; McCormac, T.; Mal, S. S.; Dickman, M. H.; Kortz, U. *Eur. J. Inorg. Chem.* **2009**, 5259−5266.

(12) (a) *CrystalClear*, 1.4.5 SP2; Rigaku and Rigaku/MSC: The Woodlands, TX, 1999. (b) Pflugrath, J. W. *Acta Crystallogr.* **1999**, *D55*, 1718−1725.

(13) Otwinski, Z.; Minor, W. Processing of X-ray Diffraction Data Collected in Oscillation Mode. In *Methods of Enzymology*; Carter, C. W. Jr., Sweet, R. M., Eds.; Macromolecular Crystallography, Part A; Academic Press: New York, 1997; Vol. *276*, pp 307−326.

(14) *CrystalStructure*, 4.0; Rigaku and Rigaku/MSC: The Woodlands, TX, 2000.

(15) Farrugia, L. J. *J. Appl. Crystallogr.* **1999**, *32*, 837−838.

(16) Sheldrick, G. M. *SHELX97, Programs for Crystal Structure Analysis*, Release 97-2; University of Göttingen: Göttingen, Germany, 1997.

(17) van der Sluis, P.; Spek, L. A. *Acta Crystallogr.* **1990**, *A46*, 194−201.

(18) Becke, A. D. *J. Chem. Phys.* **1993**, *98*, 1372−1377.

(19) Hay, P. J.; Wadt, W. R. *J. Chem. Phys.* **1985**, *82*, 270−283.

(20) (a) Barone, V.; Cossi, M. *J. Phys. Chem. A* **1998**, *102*, 1995−2001. (b) Cossi, M.; Rega, N.; Scalmani, G.; Barone, V. *J. Comput. Chem.* **2003**, *24*, 669−681.

(21) Frisch, M. J. et al. *Gaussian 09*; Gaussian, Inc.: Wallingford, CT, 2009. See Supporting Information for the complete reference.

(22) The changes in the concentrations or fractions determined by the ^{1}H, ^{29}Si, and ^{183}W NMR data were close to one another (Supporting Information, Figure S3).

(23) No inflection point was observed at 1 equiv of TBAOH for the potentiometric titration, which would be explained by closeness of the K_1 (= $[H_3{\cdot}\mathbf{I}][H_2O]/[H_4{\cdot}\mathbf{I}][OH^-]$) (eq 2) value to K_2 (= $[H_2{\cdot}\mathbf{I}][H_2O]/[H_3{\cdot}\mathbf{I}][OH^-]$) (eq 3) one.

$$H_4{\cdot}\mathbf{I} + OH^- \rightleftarrows H_3{\cdot}\mathbf{I} + H_2O \quad (2)$$

$$H_3{\cdot}\mathbf{I} + OH^- \rightleftarrows H_2{\cdot}\mathbf{I} + H_2O \quad (3)$$

(24) Crystal data of $TBA_6{\cdot}H_2{\cdot}\mathbf{I}$ for $C_{96}SiN_6O_{36}W_{10}$, fw = 3679.61, orthorhombic, space group *Pbca* (#61) with a = 17.68820(10) Å, b = 31.7087(2) Å, c = 47.8925(3) Å, V = 26861.5(3) Å^3; Z = 8; D_{calcd} = 1.820 g cm^{-3}; T = 153 K. The final refinement gave R1 = 0.1064, wR2 = 0.2765, and GOF = 1.196 for 31174 observed reflections with $I > 2\sigma(I)$.

(25) It was confirmed by ^{1}H NMR spectroscopy that the precipitates, which were obtained by addition of an excess amount of diethyl ether into the acetonitrile solution containing $TBA_4{\cdot}H_4{\cdot}\mathbf{I}$ and 3 equiv of TBAOH, were a mixture of $H{\cdot}\mathbf{I}$ (60%) and $H_2{\cdot}\mathbf{I}$ (40%).

(26) For the structurally characterized protonated lacunary POMs, terminal oxygen atoms at the lacunary sites are preferentially doubly protonated, resulting in aqua ligands: (a) Hedman, B. *Acta Chem. Scand.* **1978**, *A32*, 439−446. (b) Johansson, G.; Pettersson, L.; Ingri,

N. *Acta Chem. Scand.* **1978**, *A32*, 681−688. (c) Fang, X.; Hill, C. L. *Angew. Chem., Int. Ed.* **2007**, *46*, 3877−3880. (d) Liu, Y.-C.; Zheng, S.-T.; Yang, G.-Y. *J. Cluster Sci.* **2009**, *20*, 481−488. (e) Leclerc−Laronze, N.; Haouas, M.; Marrot, J.; Taulelle, F.; Hervé, G. *Angew. Chem., Int. Ed.* **2006**, *45*, 139−142. (f) Murakami, H.; Hayashi, K.; Tsukada, I.; Hasegawa, T.; Yoshida, S.; Miyano, R.; Kato, C. N.; Nomiya, K. *Bull. Chem. Soc. Jpn.* **2007**, *80*, 2161−2169. (g) Tourné, C. M.; Tourné, G. F. *J. Chem. Soc., Dalton Trans.* **1988**, 2411−2420. (h) Contant, R.; Thouvenot, R.; Dromzée, Y.; Proust, A.; Gouzerh, P. *J. Cluster Sci.* **2006**, *17*, 317−331. (i) Gaunt, A. J.; May, I.; Collison, D.; Helliwell, M. *Acta Crystallogr.* **2003**, *C59*, i65−i66. (j) Nsouli, N. H.; Ismail, A. H.; Helgadottir, I. S.; Dickman, M. H.; Clemente-Juan, J. M.; Kortz, U. *Inorg. Chem.* **2009**, *48*, 5884−5890. (k) Bi, L.-H.; Li, B.; Wu, L.-X.; Shao, K.-Z.; Su, Z.-M. *J. Solid State Chem.* **2009**, *182*, 83−88. (l) Ritchie, C.; Alley, K. G.; Boskovic, C. *Dalton Trans.* **2010**, *39*, 8872−8874.

(27) The ^{183}W NMR results indicate the fast proton-exchange between the two bridging oxygen atoms (i.e., O20/O22 and O25/O27).